Volume 1 | Number 1 | Jan 2013 | Pages 1–100

Journal of
Materials Chemistry A

Materials for energy and sustainability
www.rsc.org/materialsA

Li⁺

ROYAL SOCIETY
OF CHEMISTRY

ROYAL SOCIETY
OF CHEMISTRY

www.rsc.org/materialsA

Journal Name

Submicron-sized Silicon Oxycarbide Spheres as Anodes for Alkali Ion Batteries

M. Weinberger,*[a] C. Pfeifer,[b] S. Schindler,[a] T. Diemant,[c] R. J. Behm[ac] and M. Wohlfahrt-Mehrens[ab]

Submicron-sized silicon oxycarbide (SiCO) spheres were prepared in a 2-step acid/base catalyzed sol-gel process of triethoxyphenylsilane (PhTES) with subsequent carbonization at 1000 °C under argon atmosphere. To prevent the organosilica spheres from sintering during heating, small amounts of tetraethoxysilane (TEOS) were cocondensed with the carbosilane. The resulting SiCO material retains the spherical morphology (average particle diameter of around 200 – 300 nm) of the organosilica material upon heating in contrast to the SiCO obtained from pure PhTES or from the cocondensation of PhTES with methyltriethoxysilane (MTES). X-ray photoelectron spectroscopy (XPS) measurements of the SiCO spheres revealed an absolute carbon content of 41 wt%, which is only slightly lower than the carbon content of the SiCO obtained from pure PhTES with 46 wt%. Together with the O/Si ratio we determined the following composition for the SiCO spheres: $SiC_{0.3}O_{1.4} + 2.89\ C_{free}$. In order to elucidate the potential of the material as an anode material for sodium and lithium ion batteries, galvanostatic charge/discharge measurements were conducted and compared to the other SiCO materials. For the lithium system, capacities as high as 858 mAh/g at lower currents of 50 mA/g have been achieved. The spheres show significantly improved rate capability compared to the other SiCO samples. For instance, the material delivers reversible capacities of around 500 mAh/g at a specific current of 500 mA/g. It is noteworthy that the spheres show the highest first cycle coulombic efficiency (73 %) compared to the other SiCO materials (down to 51 %) prepared throughout this work, which might be attributed to the higher material utilization due to the nanoscopic morphology. The SiCO nanostructure also significantly improved the sodium insertion properties compared to bulk SiCO. For the SiCO spheres we obtained promising high reversible capacities of 200 mAh/g at lower current of 25 mA/g (1st cycle efficiency of 47 %). When increasing the currrent to 200 mA/g, the material still delivered 111 mAh/g.

Introduction

Due to their high energy densities, excellent efficiencies and a longer life span, lithium ion batteries have become the most important electrochemical energy storage devices in our daily lives. However, for areas such as electromobility, there is still considerable improvement needed to increase the energy density and rate capability of the active materials on either anode or cathode side in order to achieve higher range and improved power density, together with shortened charging times.

Currently, in most lithium ion batteries, graphite is used as anode material. It offers a theoretical capacity of 372 mAh/g, a rather small value compared to other alternatives based on, for example, silicon, which theoretically achieves up to 4200 mAh/g. However, graphite benefits from a rather low volume expansion upon cycling, a low operating potential versus lithium as well as a comparatively small irreversible capacity during the first few cycles. Other anode materials usually suffer from at least one of these aspects. In addition, the synthesis of sophisticated anode materials with improved properties compared to graphite might be much more complicated and uneconomic. One aspect in which graphite is less competitive compared to other anode materials, is its poor rate capability during lithium insertion. Considering other purely carbon based anode materials, hard carbons might be a suitable choice to overcome this issue[1-3], however, the reversible capacities in the lithium system remain still low and larger irreversible capacities as well as a more pronounced hysteresis between charge/discharge restrict its commercial application.

With sodium, graphite is practically not forming staged intercalation compounds[4]. Studies on the insertion into disordered carbons, however, revealed similar charge/discharge curves as for lithium, but due to the larger diameter of sodium, the capacities are lower in general. Stevens and Dahn were the first to report on the sodium insertion into sugar derived hard carbons[5]. 300 mAh/g could be inserted reversibly, but only at a sufficiently low C-rate of C/80. Suitable capacities at higher rates may not be achieved with conventional hard carbons, however, with modern synthetic

[a] Helmholtz Institute Ulm (HIU), Karlsruher Institute of Technology, Helmholtzstraße 11, 89081 Ulm, Germany. E-mail: manuel.weinberger@kit.edu
[b] Zentrum für Sonnenenergie- und Wasserstoffforschung (ZSW), Helmholtzstraße 8, 89081 Ulm, Germany. E-mail: margret.wohlfahrt-mehrens@zsw-bw.de
[c] Institute of Surface Chemistry and Catalysis (IOK), Ulm University, Albert-Einstein-Allee 47, 89081 Ulm, Germany
† Footnotes relating to the title and/or authors should appear here.
Electronic Supplementary Information (ESI) available: [details of any supplementary information available should be included here]. See DOI: 10.1039/x0xx00000x

approaches novel carbon materials with nanoscopic structures could be obtained, which showed improved performances at higher C-rates. Adelhelm et al. were the first to report on the high rate performance of hierarchically porous carbons[6]. Although the reversible capacities at a rate of C/5 were relatively small, with around 130 mAh/g, capacities of 100 mAh/g could still be achieved at 5C. Similar results were obtained by Kado et al. for the synthesis of an MgO templated mesoporous carbon[7]. Maier et al. report on excellent rate capability for hollow carbon nanospheres[8]. Reversible capacities of 200 mAh/g could be achieved at 100 mA/g and up to 100 mAh/g could be retained at a current of 2 A/g.

Among the lithium ion battery anode materials, silicon oxycarbides (SiCOs) are a class of comparatively less investigated materials. In the case of sodium there is even not a single report to date. The most common approaches for their synthesis use the pyrolytic conversion of polycarbosilanes at temperatures > 800°C[9-13]. The materials are composed of interconnected ceramic and carbon phases. The ceramic phase may be imagined as a silicon dioxide matrix, where oxygen is partly substituted by carbon. The free carbon phase (C_{free}) is usually observed as byproduct during the synthesis of the SiCO material and is responsible for the interesting electronic and electrochemical properties. These materials have thus gained attention with regard to their potential as a substitute for graphite as anode material in lithium ion batteries. Dahn et al. were the first to intensively characterize SiCO materials obtained from various preceramic sources with the goal to correlate the composition of the SiCO to reversible and irreversible capacities[14,15]. They found that lower irreversible capacities are obtained at higher carbon and lower oxygen contents, while larger reversible capacities of up to 900 mAh/g are obtained for larger silicon contents. Subsequent investigations of SiCO anodes by ^{7}Li and ^{29}Si solid state NMR methods revealed that lithium storage occurs on the one hand in intersticial spaces or edges of graphene layers of the free carbon phase and on the other hand in the silicon oxycarbide phase[16,17]. For the latter one it was even possible to distinguish between different silicon species with regard to their reversibility upon reaction with lithium. For instance, SiO_4 species showed partial reversibility, wheras SiO_3C species are totally irreversible with lithium.

Since ceramic processing is performed at higher temperatures, the resulting materials are often dense and show large particle sizes which may severely restrict their utilization upon electrochemical cycling as well as its rate capability. A first approach towards the realisation of a nanoscopic SiCO material was undertaken by Pradeep et al.[18] They synthesized a highly porous SiCO aerogel, which indeed delivered higher capacities at higher currents, for instance, 600 mAh/g at 360 mA/g but this was achieved at the cost of significantly higher irreversible capacities of over 100 %.

Phenyltriethoxysilane is a relatively inexpensive carbosilane and thus an attractive candidate for the preparation of preceramic precursors for the carbothermal conversion to silicon carbides and oxycarbides[19,20]. There are various reports on the sol-gel processing of PhTES to submicrometric organosilica spheres[21-25]. However, PhTES derived organosilica shows thermoplastic properties, which leads to significant coalescence during heating. Glass transition temperatures below 160 °C have been determined experimentally[24,25]. As consequence, the spherical morphology may not be retained during carbothermal treatment and large pieces of SiCO with diameters of several micrometers are obtained. It is known that the glass transition temperature may be increased by cocondensation with other monosilylated precursors such as methyltriethoxysilane[23,26], but until now, the synthesis of dense and carbon rich SiCO nanospheres with carbon contents > 40 wt% by utilizing a cocondensation approach has not been reported.

In this work we report on the successful synthesis of submicrometric SiCO spheres by a two-step acid/base processing of a mixture of phenyltriethoxysilane (PhTES) with tetraethoxysilane (TEOS). The substitution of 20 mol% of PhTES with TEOS suppressed the sintering of the organosilica cocondensate at higher temperatures. The novel material is compared to SiCOs derived from pure PhTES and a cocondensate of PhTES with methyltriethoxysilane (MTES) which upon pyrolysis either do not show spherical morphologies or an intermediate structure between spheres and sintered domains. In the first part of the paper we will analyse and compare the structural and compositional features of the SiCO materials. This is followed by a detailed investigation of the potential of these materials as anode in lithium and sodium ion batteries by galvanostatic charge/discharge measurements.

Experimental section

Materials synthesis

All chemicals were used as received. In a typical synthesis 2 g of 0.01 M aqueous HCl solution was further diluted with 5.5 g of demineralized water and 15.17 g of absolute ethanol. To this solution 21 mmol of silanes were added and the solution was stirred for 7 h. Three systems were investigated. The first material was derived from pure phenyltriethoxysilane (PhTES, Aldrich, 98%). The second system consists of a mixture of PhTES and methyltriethoxysilane (MTES, Alfa Aesar, 98%) in a molar composition of 4:1 (17 mmol of PhTES and 4 mmol of MTES) and the third system was a cocondensate of PhTES and tetraethoxysilane (TEOS, Aldrich, ≥99%) with the same ratio. For following discussions, the three systems will be denoted as follows: the first as OS_Ph, the second as OS_Ph_M and the third as OS_Ph_T In the next step of the synthesis, 10 ml of aqueous ammonium hydroxide solution (28 wt%) were further diluted to a total of 70 ml with demineralized water. The solution was stirred and the precursor sol was quickly added. A milky suspension rapidly formed which was further stirred for 48 h. The organosilica spheres are separated via centrifugation with a Compactstar CS4 from VWR (6500 rpm, 15 min). After a first centrifugation cycle the spheres were washed with demineralized water followed by a second centrifugation cycle. Subsequently, the spheres were dried at room temperature (RT)

in vacuum overnight. For carbonization, the spheres were placed in an alumina crucible and heated in a modified CWF1100 oven from Carbolite up to 1000 °C with a heating rate of 10 °C/min. The samples were kept at the final temperature for 2 h. Ceramic yields are around 80 wt%. Prior to heating, three evacuation/purging cycles were applied to remove air and moisture from the system. The notation of the samples changed as follows: OS_Ph to SiCO_Ph, OS_Ph_M to SiCO_Ph_M and OS_Ph_T to SiCO_Ph_T.

Materials characterisation

The particle morphology of organosilica and silicon oxycarbide materials were imaged with Scanning Electron Microscopy (SEM) using a LEO 1530 VP with a LEO Gemini field emission column. SiCO samples were coated with a 4 nm thin layer of Pt. SEM images were obtained with an in-lens detector at an accelerating voltage of 4 kV and a working distance of 6 mm.

Nitrogen sorption measurements were performed at 77 K on a Quadrasorb SI (Quantachrome). Organosilica samples were outgassed in vacuum at RT (to avoid sintering), SiCO samples at 150 °C prior to the measurements. The specific surface areas were determined by application of the Brunauer/Emmett/Teller (BET) equation in the lower relative pressure range (p/p0 = 0.05−0.15), where the isotherm behaves in a linear fashion.

The elemental composition of the surface region of the SiCO samples was determined by X-ray photoelectron spectroscopy (XPS) measurements using a Physical Electronics PHI 5800 ESCA system. The measurements were performed using monochromatized Al K_α radiation (13 kV, 250 W) at a detection angle of 45° and pass energies of 93.9 eV and 29.35 eV for the survey and detail scans, respectively. If necessary, an electron flood gun was used for sample neutralization. The main C(1s) peak was set to 284.6 eV for binding energy calibration. In order to remove surface contaminations the samples were sputtered for 2 minutes (sputter rate ~1nm/min, 1 μA, 5 kV). XPS measurements were performed before and after sputtering.

Electrochemical characterisation

SiCO samples were finely ground in an agate mortar. 250 mg of the SiCO powders were mixed with 31.25 mg of Timcal Super P carbon black (CB) and 0.531 g of a mixture of 500 mg PVDF binder (MTI corporation) and 8 g 1-Methyl-2-pyrrolidinone (NMP, Aldrich, ≥99%). This results in an dry electrode layer composition for SiCO/CB/PVDF of 80/10/10 (in wt%). To make the slurry less viscous an additional 100 mg of NMP was added. The slurries were coated onto copper foil (SE-Cu58, 10 μm thick, Schlenk Metallfolien GmbH & Co KG) with a wet film thickness

of 200 μm using an Elcometer casting knife film applicator and a Coatmaster 509 MC from Erichsen. The resulting active material loadings are around 3-4 mg/cm². Circular electrodes with a diameter of 12 mm were punched out of the electrode sheets. CR2032 button cells were fabricated within an argon filled glovebox. A glass fiber filter paper (GF/A, Whatman) was used as separator, a lithium metal foil (Alfa Aesar, 99.9%) or pressed and punched pieces of dry sodium (Aldrich) served as counter electrodes. Either 100 μl of 1M LiPF$_6$ in a 50/50 (v/v) mixture of ethylene carbonate and dimethyl carbonate (Aldrich, battery grade) or 1M NaPF$_6$ (Alfa Aesar, 99+%, dried at 60 °C in vacuum) in propylene carbonate (Selectilyte, BASF) were applied as electrolyte. Galvanostatic charge/discharge measurements were performed using a VMP3 galvanostat from BioLogic Science Instruments. For lithium, rate capability measurements at specific currents of 50, 100, 200, 500, 1000, 2000 and 3000 mA/g were carried out on all three samples. Cycle stability measurements were performed on sample SiCO_Ph_T at a specific current of 500 mA/g. In order to create a stable SEI, however, a current of 100 mA/g was applied for the first two cycles. The voltage window in the lithium system was set between 0.005 and 3 V for rate capability and cycle stability measurements. For sodium, almost the same rate capability program was used, however, an additional cycling at a lower current of 25 mA/g was added. The same voltage window as in the lithium system was used. Concluding cycle stability measurements for SiCO_Ph_T were performed at 25 mA/g. In that case, however, the upper cut-off voltage was reduced to 2 V to provide more stable cycling.

Results and discussion

A two-step sol-gel processing was applied to synthesize the different preceramic organosilica precursors. The first step comprises the hydrolysis of the silane mixtures in water/ethanol mixtures under acidic conditions. No matter which precursor system was investigated, the silanes were always completely soluble under these conditions. Within 7 h the precursors will undergo hydrolysis and condensation to smaller oligomeric species. The sol is then quickly added to an alkaline environment, where silca-based precursors tend to favor the formation of denser structures. Nucleation and growth take place almost immediately after the addition of the sol. As a result, we observe for all three systems OS_Ph, OS_Ph_M and OS_Ph_T the formation of spherical particles with average diameters between 200 – 300 nm. Fig. 1a contains a representative SEM picture of sample OS_Ph_T. As expected for

Tab. 1. Elemental composition of silicon oxycarbide samples and BET surface areas for organosilica and silicon oxycarbide samples

Sample	Sol-gel precursor		Absolute carbon content [wt%]	Molar O/Si ratio	Free carbon content [wt%]	SiCO formula $SiO_{2-x}C_{x/2} + yC_{free}$	BET surface areas [m²/g]	
	Compounds	Molar ratio					Organosilica	Silicon oxycarbide
SiCO_Ph	PhTES	---	46	1.31	42	$SiC_{0.34}O_{1.31} + 3.49\ C_{free}$	15	n/a
SiCO_Ph_M	PhTES/MTES	80/20	40	1.42	36	$SiC_{0.29}O_{1.42} + 2.84\ C_{free}$	13	n/a
SiCO_Ph_T	PhTES/TEOS	80/20	41	1.4	37	$SiC_{0.3}O_{1.4} + 2.89\ C_{free}$	16	64

a (co)condensation under basic conditions, the surface areas determined by nitrogen sorption measurements (see tab. 1) are below 20 m²/g, indicating the formation of dense organosilica particles.

The spheres were then subjected to carbonization at 1000°C under inert gas atmosphere. The three systems showed significant differences with regard to structural stability of the spherical particles during thermal treatment. As expected, sample SiCO_Ph shows complete sintering of the particles, which can be seen in fig. 1d. In contrast to the other materials, SiCO_Ph lost its powder appearance during carbonisation and instead formed a solid spongelike block with a shiny graphitic surface. It is well known from literature that organosilicas solely derived from PhTES show thermoplastic properties with low glass transition temperatures[24,25] and it is thus not surprising that the system is not stable under these conditions. Tatsumisago et al. investigated the copolymerisation of alkyltrialkoxysilanes with PhTES in order to elucidate the influence on the thermal properties[23]. In their case, the substitution of 20 mol% of PhTES by MTES lead to a significant increase of the glass transistion temperature from 160 to 380 °C. In their work they applied ex-situ SEM investigations on thermally treated samples to determine glass transition

temperatures, so these values have to be considered as a rough estimate. Their SEM investigations of the sample treated at 380 °C however, revealed that the thermal treatment has not lead to a complete sintering of the particles. Instead, the particles tend to form a coarse network of partly sintered structures. A similar behaviour is observed for sample SiCO_Ph_M (fig. 1c). Obviously, cocondensation has a significant influence on the thermoplastic properties of polyphenylsilsesquioxanes (PPSQ), most likely due to the decreased flexibility of the ladder-like chains of the PPSQ by increased crosslinking induced by the trialkoxysilane. This lead us to the question whether it is possible to further stiffen the PPSQ network by introducing TEOS, which has four hydrolysable groups and thus could lead to an even higher degree of crosslinking. Fig 1b. shows an SEM image of the resultant SiCO_Ph_T material. The spheres have been retained by the thermal treatment, no sintering is observed in the system. The size of the particles did not change significantly during the conversion of the organosilica to the SiCO matrix. However, a closer look reveals small notches on the particles surfaces which might occur by breaking the particles apart. It is likely that during thermal treatment a partial sintering occurs between two particles attached to each other. It has to be noted that we also tried to reduce the amount of
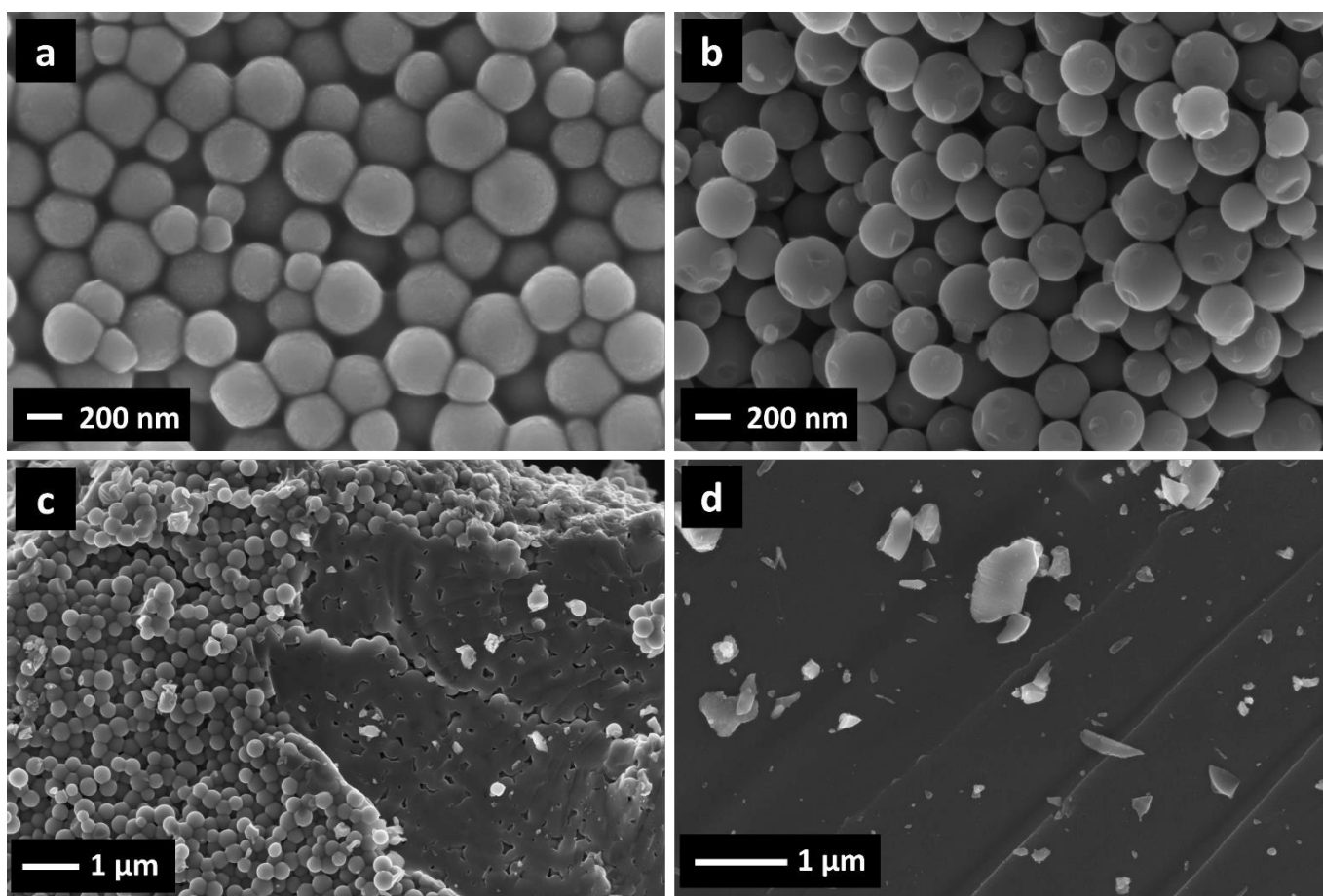

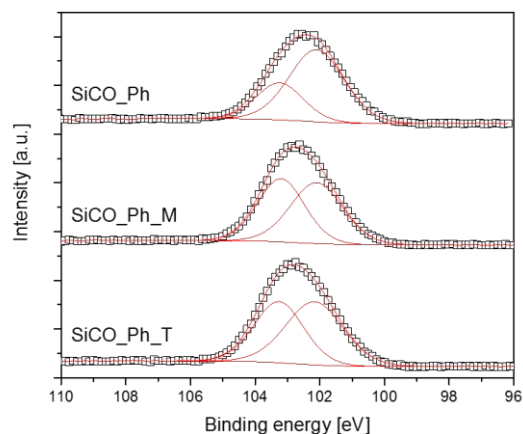**Fig. 1.** SEM images for a) OS_Ph_T, b) SiCO_Ph_T, c) SiCO_Ph_M and d) SiCO_Ph

Fig. 2. Si2p XPS spectra for argon sputtered SiCO samples. Rectangles represent experimental data, red straight lines the corresponding fit curves.

TEOS. However, when applying a molar composition for PhTES to TEOS of 90 mol% to 10 mol%, a material was obtained, which was from a structural point of view similar to SiCO_Ph_M.

The elemental composition of SiCO materials was determined by X-ray photoelectron spectroscopy (XPS). The results are also summarized in tab. 1. The SiCO spheres show an absolute carbon content of 41 wt% which is only slightly lower than the carbon content obtained for sample SiCO_Ph with 46 wt%. Obviously, the substitution of 20 mol% of PhTES by TEOS did not lead to a decrease of carbon content by 20 wt%, thus the chemical composition of the preceramic organosilica precursor might have a significant influence on the final SiCO composition. A more oxygen deficient material was obtained in the case of SiCO_Ph, indicating the formation of a slightly larger amount of carbidic silicon species. This is also confirmed by a detailed look at the Si2p spectra in fig. 2. The spectra of all three samples can be fitted by two peaks at 103.2 eV (Si in SiO_4 groups) and 102.1 eV (Si in oxycarbide).[27] For samples SiCO_Ph_M and SiCO_Ph_T both peaks have roughly the same intensity, while the peak assigned to oxycarbide species dominates/overweighs in the case of sample SiCO_Ph. However, care has to be taken when discussing the results from the sputtered samples with regard to absolute values, since preferred sputtering of lighter elements might lead to an overestimation of the real silicon content. It has also to be noted that samples, which are not argon sputtered show significantly higher O/Si ratios of around 2.15 compared to 1.3-1.4 for the sputtered samples, independently from the precursor composition. Since XPS is a surface sensitive technique and thus restricted to a penetration depth of 10 nm, we conclude that the surfaces of the SiCO materials show higher O/Si ratios probably due to a larger silica concentration and/or oxidized free carbon.

Nitrogen sorption measurements were also conducted on the SiCO samples. Although 500 mg portions were used for the measurements, no meaningful surface areas could be detected for samples SiCO_Ph and SiCO_Ph_M, indicating rather low surface areas what can be ascribed to the densification of the
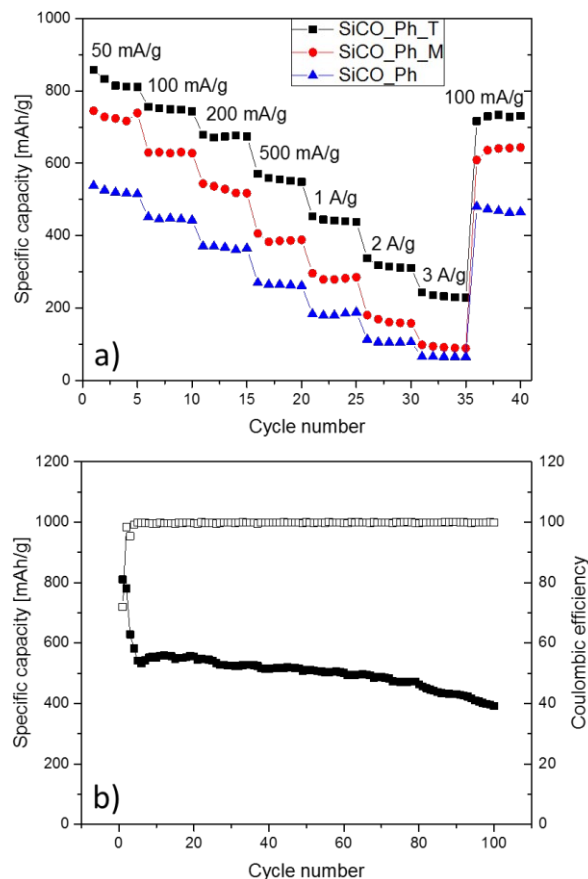

Fig. 3. a) Rate capability measurements for all SiCO samples and b) cycle stability measurement at a current of 500 mA/g for SiCO_Ph_T.Electrolyte: 1M $LiPF_6$ dissolved in EC/DMC (50/50, v/v). The voltage window in both cases was set to 0.005 - 3 V. Active material loadings [mg/cm^2]: a) SiCO_Ph_T = 3.5, SiCO_Ph_M = 4.6, SiCO_Ph = 4.3; b) 3.7.
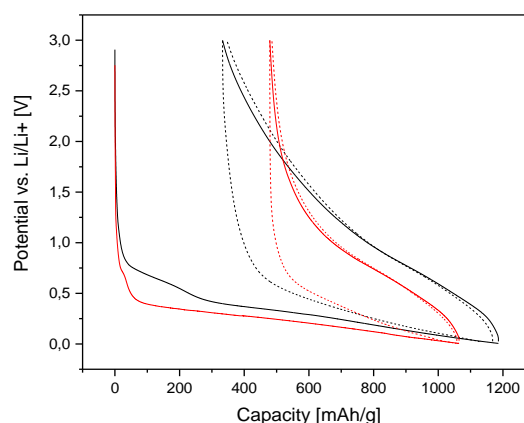

Fig. 4. Charge/Discharge curves for samples SiCO_Ph (red) and SiCO_Ph_T (black) in the lithium system. The straight lines are associated to the first cycle, the dotted lines to the second cycles. Electrolyte: 1M $LiPF_6$ dissolved in EC/DMC (50/50, v/v). Voltage window: 0.005 – 3V. Active material loadings [mg/cm^2]: SiCO_Ph = 4.3, SiCO_Ph_T = 3.7.
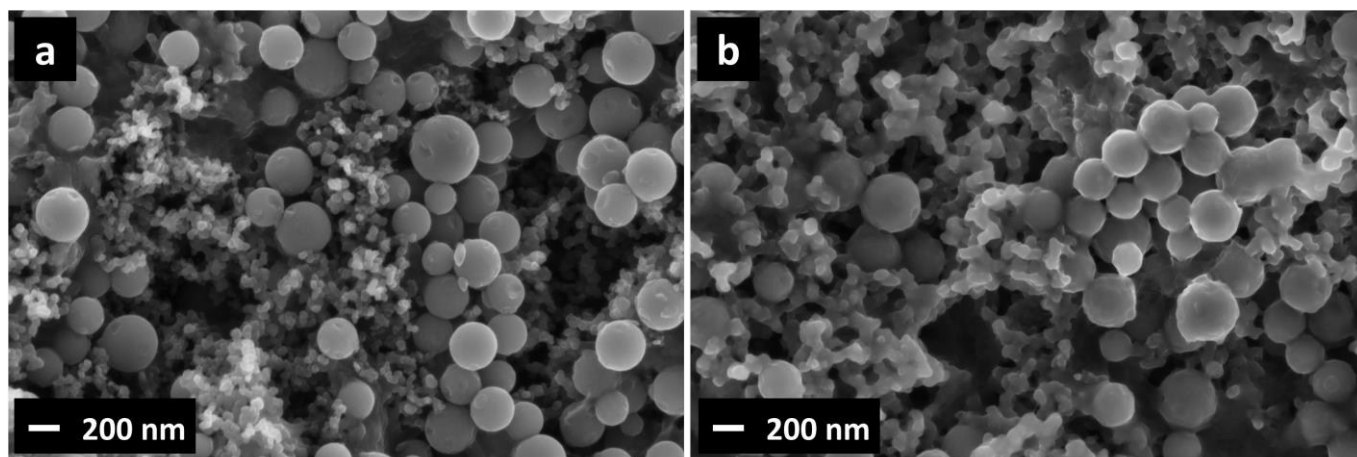
Fig. 5. SEM images for a) the as-prepared electrode of SiCO_Ph_T and b) the cycled electrode of fig. 3 b). The measurement was performed with the discharged electrode. The smaller particles consist of carbon blacks as conductive additives.

materials during thermal treatment. SiCO_Ph_T, however, showed a small BET surface area of 64 m^2/g, which might probably be attributed to the formation of free carbon on the surface of resulting nanospheres.

To test the silicon oxycarbides as anode materials in alkali ion batteries, galvanostatic charge/discharge measurements were performed. The upper plot in fig. 3 contains rate capability data for all three samples in the lithium system. As expected, sample SiCO_Ph shows lower discharge capacities due to the dense and large aggregates which are formed during pyrolysis. Capacities of 500 mAh/g are only realized at low current of 50 mA/g and at 500 mA/g the capacities are decreased to around 250 mAh/g. However, the reduction of the particle size into the submicrometer range significantly enhances the electro-chemical performance of SiCO. Capacities of above 850 mAh/g may be obtained for sample SiCO_Ph_T at a current of 50 mA/g and if the current is increased to a value as high as 3 A/g, still capacities above 200 mAh/g may be achieved. The improved rate capability may be explained by shortened diffusion paths for lithium ions due to the nanoscopic dimensions of the spheres.

The first two charge/discharge curves of SiCO_Ph_T at a current of 50 mA/g are illustrated in fig 4. Pradeep et al. have recently investigated the performance of silicon oxycarbide aerogels as lithium ion battery anode materials[18]. The nanoporous framework significantly enhanced capacities and rate capability, however, the charge/discharge curves showed a huge hysteresis, which led to the problem, that almost a third of the whole capacity could only be extracted above 2 V. Although not as distinct as in their work, sample SiCO_Ph_T seems to behave in a similar way. The comparison of sample SiCO_Ph, which represents a typical dense SiCO, with sample SiCO_Ph_T clearly shows a more pronounced hysteresis for the nanoscopic material. Raj et al. have investigated the hysteresis for SiCO materials in more detail[28]. They came to the conclusion that the hysteresis in SiCOs is to a large extent of a thermodynamic origin, rather than a kinetic one. As a reason for this, they state that lithium ions within the SiCO

anode/electrolyte interface have a higher electrochemical potential than lithium ions dissolved within the electrolyte. In case of the nanoscopic SiCOs, the surface area is much higher than for bulk materials and thus there will be a higher concentration of lithium ions in the SiCO/electrolyte interface, what might explain increasing hysteresis compared to bulk SiCO.

Based on the charge/discharge curves, the differential capacity plots are illustrated in fig S1. The first cycle insertion for both samples shows a peak at around 0.4 V, which might be attributed to SEI formation. It is also obvious that the extraction of lithium ions occurs over a broader potential range for the nanoscopic SiCO.

In the lower plot of fig. 3, a cycle stability measurement for sample SiCO_Ph_T at a current of 500 mA/g is shown. The system shows a promising behaviour since 400 mAh/g may be maintained after 100 cycles. Except for the first few cycles, the coulombic efficiencies are always well above 99.5 %. Excellent efficiencies are also observed, when the material is cycled at the other currents. Fig. 5 shows corresponding ex-situ SEM images of the cycled electrode (from fig. 3 b) compared to the as-prepared one. The spherical shape of the particles as well as its size distribution remain stable. However, a closer look at the surfaces of the cycled spheres reveal significant deposition probably due to SEI formation or electrolyte decomposition during cycling. More detailed investigations on the surface reactions will be reported in the future.

A very remarkable feature of sample SiCO_Ph_T is its significantly lower irreversible capacity during the first cycle in contrast to the other two samples. In tab. 2 the charge/discharge capacities and corresponding efficiencies during first cycle are summarized. Sample SiCO_Ph shows a first coulombic efficiency of only 51 %, whereas for SiCO_Ph_T the efficiency increases to 73 %. Normally, one would expect a decrease of efficiency with an increase of surface area. In our case, however, the transition to a nanoscopic and spherical morphology seems to have an oppositional effect. One possible explanation for this behaviour might come from a higher

Tab. 2. First cycle capacities and corresponding efficiencies

Sample	Alkali metal	Spec. Current [mA/g]	$C_{insertion}$ [mAh/g]	$C_{extraction}$ [mAh/g]	$C_{irreversible}$ [mAh/g]	Efficiency [%]
SiCO_Ph	Li	50	1064	538	526	51
	Na	25	281	83	198	30
SiCO_Ph_M	Li	50	1114	745	369	67
SiCO_Ph_T	Li	50	1177	858	319	73
	Na	25	399	188	211	47

materials utilisation during lithium extraction. In fact, the SiCO samples show more or less the same initial insertion capacity, but the nanoscopic spheres might facilitate subsequent extraction due to enhanced ion diffusion, for instance. The synthesis of the spheres might also have led to a higher silica concentration at the surface of the spheres, which in turn may result in some kind of passivation which reduces irreversible losses. Further studies on this phenomenon are already in progress and will be reported in future publications.

High capacity SiCO materials usually fulfil the so-called "nanodomain model", in which mixed-bond silicon tetrahedra and free carbon form a nanoscopic and cocontinuous network[14,29]. These SiCO materials may be found in a quite limited area of the Si-C-O ternary phase diagram. A comparison of the chemical composition of our materials with the literature clearly shows that all of our materials must lie in this nanodomain area. For SiCO_Ph_T we find indeed samples in the cited literature with similar chemical composition, which show almost the same capacities and efficiencies. With regard to the chemical composition, samples SiCO_Ph_M and SiCO_Ph_T seem to be almost identical, however the capacities are higher for the latter one. Thus, the morphology of the materials seems to have a significant influence on the electrochemical properties. The bulk sample SiCO_Ph shows an even higher deviation from literature due to lower capacities and effeciencies. A possible explanation for this deviation might lie in different synthesis techniques for the preceramic polymers. Whereas our approach utilizes only sol-gel processing for precursor synthesis, the cited literature is using a combination of a sol-gel approach with catalytic cross-linking of vinyl moieties. It is well known in SiCO literature that the chemical composition of the preceramic precursor strongly affects the SiCO composition with regard to the distribution of the mixed-bond silicon tetrahedra and it is thus not surprising that the electrochemical properties will differ[13].

Since our materials showed interesting properties in the lithium system, we also wanted to determine their performance as anodes in sodium ion batteries. The first two charge/discharge curves at a specific current of 25 mA/g for samples SiCO_Ph and SiCO_Ph_T are shown in fig. 6. Charge/discharge characteristics for the first cycle are also summarized in tab. 2. There are significant differences compared to the lithium system. We observed increased
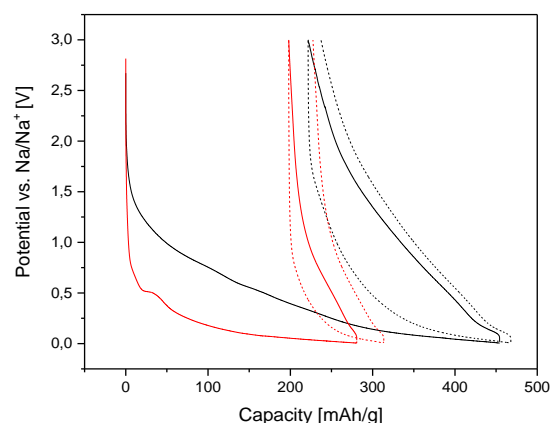
Fig. 6. Charge/Discharge curves for samples SiCO_Ph (red) and SiCO_Ph_T (black) in the sodium system. The straight lines are associated to the first cycle, the dotted lines to the second cycles. Electrolyte: 1M $NaPF_6$ dissolved in PC. Voltage window: 0.005 − 3V. Active material loadings [mg/cm²]: SiCO_Ph = 4.4, SiCO_Ph_T = 3.7.
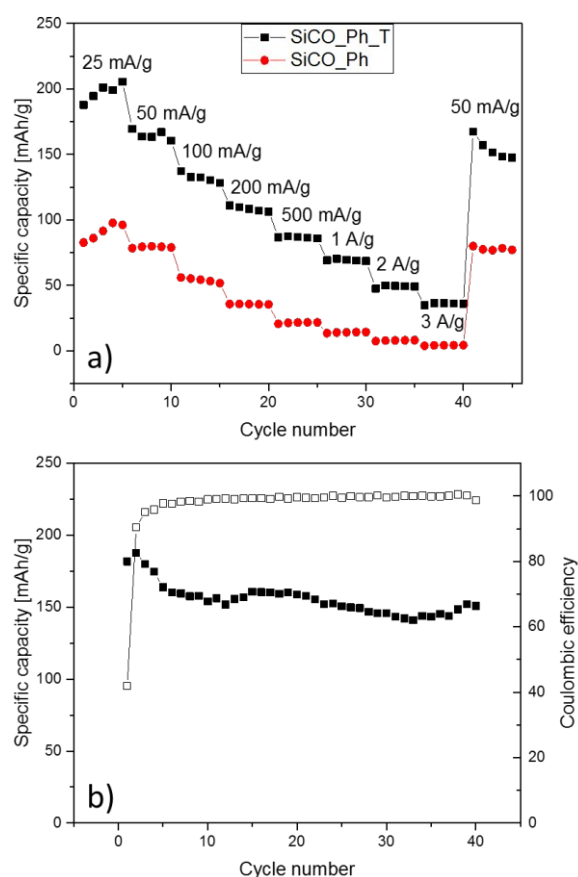
Fig. 7. a) Rate capability measurements for SiCO_Ph and SiCO_Ph_T samples and b) cycle stability measurement at a current of 25 mA/g for SiCO_Ph_T. Electrolyte: 1M $NaPF_6$ dissolved in PC. The voltage window for a) was set to 0.005 - 3 V, for b) to 0.005 − 2 V. Active material loadings [mg/cm²]: a) SiCO_Ph_T = 3.7, SiCO_Ph = 4.4; b) 3.2.

irreversible capacities and decreased discharge capacities in general. For sample SiCO_Ph the efficiency is reduced to 30 % and the first discharge capacitiy amounts to only 83 mAh/g. SiCO_Ph_T has a higher efficiency of 47 % and a first discharge capacity of 188 mAh/g, which is more than twice the capacity of the dense SiCO material. Although not acceptable for application, the efficiency is still much higher as the ones reported for other nanostructured carbon materials with comparable capacities. Efficiencies below 30 % are often observed[6,7]. A more distinct hysteresis for SiCO_Ph_T compared to SiCO_Ph is also observed in the sodium system. Complementary differential capacity plots of the charge/discharge curves in fig. S1 show in principle the same trends as for the lithium system.

SiCO_Ph_T shows promising rate capability (fig. 7a). At 500 mA/g almost 100 mAh/g may be obtained, which is for a carbon based anode a comparatively good value in the sodium ion battery system. Further cycle stability measurements for sample SiCO_Ph_T are shown in the lower plot of fig. 7. To improve cycle stability, we had to decrease the upper cut-off voltage to 2 V, else we observe random failure of the cells between 2–3 V from time to time. The sample shows stable cycling. Efficiencies above 99% are reached with continuous cycling. After 40 cycles still 150 mAh/g may be extracted. It has to be said, that these are only first results. The electrode processing and the electrolyte are by no means optimized, yet. Thus, further improvement of the cycle stability in both lithium and sodium system is expected by utilizing more advanced binders such as carboxymethylcellulose or by adding electrolyte additives such as fluoroethylene carbonate (FEC) in order to suppress capacity fading by stabilizing the solid electrolyte interface.

The transition from bulk SiCO to nanospheres has shown to significantly increase the capacities in the lithium and sodium ion battery systems. Obviously, larger surface areas and reduced diffusion paths have a beneficial effect, however, several more complex questions remain unanswered. Subsequent studies of this system have to address how the lower irreversible capacities of the nanospheres can be explained. It will also be interesting to learn more about the chemical composition of the spheres, in fact, how the different chemical species, such as free carbon, carbidic silicon and silica contribute to reversible and irreversible capacities. Another interesting aspect will be to investigate mechanistic differences between sodium and lithium ion storage. Especially in the sodium system it will be very interesting to see if the silicon oxycarbide phase is active for sodium storage or not. Since silicon is known to only hardly undergo alloying with sodium, silicon oxycarbides may thus provide a back door for utilizing silicon as possible anode material for sodium ion batteries in the future.

Conclusions

Submicrometric silicon oxycarbide (SiCO) spheres were synthesized by a facile two-step acid-base sol-gel processing of a mixture of phenyltriethoxysilane (PhTES) and tetraethoxysilane (TEOS) followed by subsequent carbonisation under inert gas atmophere. SEM investigations showed that TEOS successfully suppressed the coalescence of the spherical organosilica particles upon thermal treatment. Sorption measurements revealed a BET surface area of 64 m^2/g which can be assigned to the formation of a small amount of micropores during pyrolysis. In contrast, the surface area for SiCO obtained solely from PhTES was too small to be detected by the BET method. Elemental analysis revealed an absolute carbon content of 41 wt%. Together with XPS measurements of the O/Si ratio we could deduce the following formula: $SiC_{0.3}O_{1.4}$ + 2.89 C_{free}. Galvanostatic charge/discharge measurements in the lithium as well as in the sodium ion battery system revealed the materials promising response towards repeated charging/discharging. In the lithium system large capacities of up to 858 mAh/g could be achieved at a slower current of 50 mA/g. Due to the nanoscopic dimensions, the material is able to achieve also higher capacities at significantly higher rates. For instance, capacities above 500 mAh/g can be achieved at a specific current of 500 mA/g even at high active material loading of 3.7 mg/cm^2. The SiCO material was also investigated as potential anode material in sodium ion batteries. The material provided around 200 mAh/g at a lower current of 25 mA/g, which is in the light of a first report a very promising value.

Acknowledgements

Notes and references

1 Z. Guo, C. Wang, M. Chen, M. Li, Int. J. Electrochem. Sci., 2013, **8**, 2702 – 2709 A
2 E. Buiel, J. R. Dahn, Electrochim. Acta, 1999, **45**, 121 – 130
3 J-H. Kim, J-S. Kim, Y-G. Lim, J-G. Lee, Y-J. Kim, J. Power Sources, 2011, **196**, 10490 – 10495
4 J. Sangster, J.Phase Equilib. Diffus., 2007, **28**, 571 – 579
5 D. A. Stevens, J. R. Dahn, J. Electrochem. Soc., 2000, **147**, 1271
6 S. Wenzel, T. Hara, J. Janek, P. Adelhelm, Energy Environ. Sci., 2011, **4**, 3342
7 Y. Kado, Y. Soneda, N. Yoshizawa, ECS Electrochem. Lett., 2015, **4**, A22 – A23
8 K. Tang, L. Fu, R. J. White, L. Yu, M-M. Titirici, M. Antonietti, J. Maier, Adv. Energy Mater., 2012, **2**, 873 – 877
9 F. Babonneau, K. Thorne, J. D. Mackenzie, Chem. Mater., 1989, **1**, 554
10 G.D. Sorarù, Q. Liu, L. V. Interrante, T. Apple, Chem. Mater., 1998, **10**, 4047
11 C. Vakifahmetoglu, V. Presser, S-H. Yeon, P. Colombo, Y. Gogotsi, Microporous Mesoporous Mater., 2011, **144**, 105 – 112
12 A. Meier, M. Weinberger, K. Pinkert, M. Oschatz, S. Paasch, L. Giebler, H. Althues, E. Brunner, J. Eckert, S. Kaskel, Microporous Mesoporous Mater., 2014, **188**, 140 – 148
13 M. Weinberger, S. Puchegger, T. Fröschl, F. Babonneau, H. Peterlik, N. Hüsing, Chem. Mater., 2010, **22**, 1509 – 1520
14 W. Xing, A.M. Wilson, K. Eguchi, G. Zank, J. R. Dahn, J. Electrochem. Soc., 1997, **144**, 2410 – 2416

15 17W. Xing, A. M. Wilson, G. Zank, J. R. Dahn, Solid State Ion., 1997, **93**, 239 – 244

16 H. Fukui, H. Ohsuka, T. Hino, K. Kanamura, ACS Appl. Mater. Interfaces, 2010, **2**, 998 – 1008

17 X. Liu, M-C. Zheng, K. Xie, J. Power Sources, 2011, **196**, 10667 – 10672

18 V. S. Pradeep, D. G. Ayana, M. Graczyk-Zajac, G. D. Sorarù, R. Riedel, Electrochim. Acta, 2015, **157**, 41 – 45

19 C. Liu, H. Z. Chen, S. Komarneni, C. G. Pantano, J. Porous. Mater., 1996, **2**, 245 – 252

20 P. Gupta, W. Wang, L-S. Fan, Ind. Eng. Chem. Res., 2004, **43**,4732 – 4739

21 L. A. S. De A. Prado, E. Radovanovic, H. O. Pastore, I. V. P. Yoshida, I. L. Torriani, J. Polym. Sci. A Polym. Chem., 2000, **38**, 1580 – 1589

22 K. Takahashi, K. Tadanaga, A. Hayashi, A. Matsuda, K. Katagiri, M. Tatsumisago, J. Nanosci. Nanotechnol. 2007, **7**, 3307 – 3312

23 J. Macan, K. Tadanaga, M. Tatsumisago, J. Sol-Gel Sci. Technol., 2010, **53**, 31 – 37

24 K. Takahashi, K. Tadanaga, A. Matsuda, A. Hayashi, M. Tatsumisago, J. Sol-Gel Sci. Technol., 2007, **41**, 217 – 222

25 K. Takahashi, K. Tadanaga, A. Matsuda, A. Hayashi, M. Tatsumisago, J. Ceram. Soc. Japan, 2007, **115**, 131 – 135

26 S. Diré, V. Tagliazucca, L. Salvadori, G. D. Sorarù, J. Am. Ceram. Soc., 2011, 94, 3819 – 3824

27 G. D. Sorarù, G. D'Andrea, A. Glisenti, Mater. Lett., 1996, **27**, 1 – 5

28 D. Ahn, R. Raj, , J. Power Sources, 2010, **195**, 3900 – 3906

29 P. E. Sanchez-Jimenez, R. Raj, J. Am. Ceram. Soc., 2010, **93**, 1127 - 1135
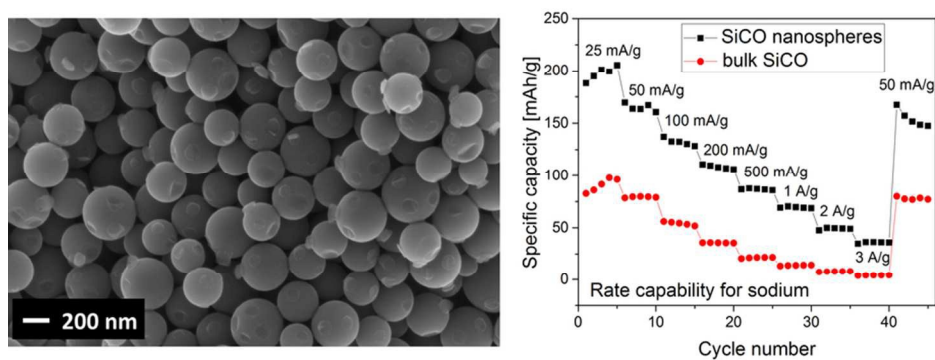
Silicon oxycarbide nanospheres were synthesized as an anode for sodium and lithium ion batteries. In the sodium system the material delivers high capacities of up to 200 mAh/g at 25 mA/g.
83x33mm (300 x 300 DPI)